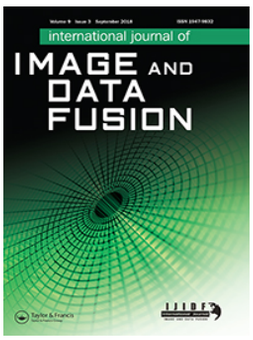

International Journal of Image and Data Fusion

ISSN: 1947-9832 (Print) 1947-9824 (Online) Journal homepage: https://www.tandfonline.com/loi/tidf20

Photogrammetric refinement of LiDAR-derived building roof contours

Aluir Porfírio Dal Poz

To cite this article: Aluir Porfírio Dal Poz (2018) Photogrammetric refinement of LiDAR-derived building roof contours, International Journal of Image and Data Fusion, 9:3, 209-221, DOI: 10.1080/19479832.2018.1440438

To link to this article: https://doi.org/10.1080/19479832.2018.1440438

INTERNATIONAL JOURNAL OF IMAGE AND DATA FUSION
2018, VOL. 9, NO. 3, 209–221
https://doi.org/10.1080/19479832.2018.1440438

Taylor & Francis
Taylor & Francis Group

RESEARCH ARTICLE

Photogrammetric refinement of LiDAR-derived building roof contours

Aluir Porfírio Dal Poz

Department of Cartography, São Paulo State University, Presidente Prudente, Brazil

ABSTRACT

In this paper, a photogrammetric method is proposed for refining 3D building roof contours extracted from airborne Light Detection And Ranging (LiDAR) data. It is assumed that LiDAR-derived planar faces of roofs are potentially accurate, while LiDAR-derived building roof contours are not well defined. First, polygons representing building roof contours are extracted from a high-resolution aerial image. Second, straight-line segments delimitating each building roof polygon are projected onto the corresponding LiDAR-derived roof planes by using a line-based photogrammetric model. Finally, refined 3D building roof contours are reconstructed by connecting every pair of photogrammetrically projected adjacent straight lines. The obtained results showed that the proposed approach worked properly, meaning that the integration of image data and LiDAR data allows better results to be obtained, when compared to the results generated by using only LiDAR data.

ARTICLE HISTORY
Received 10 September 2017
Accepted 2 February 2018

KEYWORDS
LiDAR; photogrammetry; line-based photogrammetric model; building roof contour

1. Introduction

Building extraction methods are very important in the context of spatial data capture and updating for GIS applications. These methods may be classified into three categories according to the kind of input data (Gilani *et al*. 2015): methods using **Li**ght **D**etection **A**nd **R**anging (LiDAR) data, using photogrammetric data, and combining LiDAR and photogrammetric data.

Methods based on photogrammetric data have been proposed for over 20 years. Fua and Hanson (1987) presented a method for outlining complex rectilinear buildings in aerial images. Müller and Zaum (2005) used a region-growing segmentation method and a classification procedure for detecting building in aerial images. Akçay and Aksoy (2008) combined spectral and structural information for separating building and other objects. Ferraioli (2010) used Markov Randon Field (MRF) for building edge detection. Sirmaçek and Ünsalan (2011) also presented a probabilistic approach but for detecting buildings in aerial and satellite images. In Dennis Dahlke *et al*. (2015), a method for 3D building reconstruction is proposed. A dense point cloud is first generated by photogrammetrically processing high-resolution oblique and vertical aerial images, followed by façade, roof, and overhang modelling. Argyridis and Argialas (2016) proposed a multi-

CONTACT Aluir Porfírio Dal Poz aluir@fct.unesp.br 305 R. Roberto Simonsen, Presidente Prudente, Brazil

scale object-based image analysis that integrated deep learning classification and fuzzy ontologies, aiming at detecting building changes in suburban areas.

Methods for building detection or extraction from LiDAR data can be grouped into the following categories: building detection, building roof contour extraction, building roof extraction, and building model extraction. Building detection is performed using a digital surface model (DSM) (Matikainen *et al*. 2003), a normalised DSM (Tóvari and Vögtle 2004), or a LiDAR point cloud (Tarsha-Kurdi *et al*. 2006). Building roof contour extraction usually involves the detection of irregular building roof contours, which are further subjected to a regularisation process (Sampath and Shan 2007, Wei 2008, Perera *et al*. 2012). Galvanin and Dal Poz (2012) only addressed the detection of irregular building roof contours. Building roof extraction uses segmentation methods to group LiDAR point cloud data into planar faces, requiring some kind of homogeneity criterion such as approximate height similarity and/or approximate normal vector similarity (Rottensteiner *et al*. 2005, Sampath and Shan 2010). Building model extraction usually involves building detection, building roof contour extraction, and building roof extraction (Henn *et al*. 2013, Sun and Salvaggio 2013, Chen *et al*. 2014). Haala and Kada (2010) provided an extensive and comprehensive review of the state of the art of 3D building reconstruction methods and their principles using not only LiDAR data but also airborne and terrestrial images.

Methods based on the combination between photogrammetric and LiDAR data seek to take advantage of the synergy between both data sources. Haala and Brenner (1999) combined multispectral imagery and Digital Elevation Model (DEM) derived from LiDAR data (in short, LiDAR-derived DEM) for separating buildings from vegetation. In Sohn and Dowman (2003), buildings are first extracted from both Ikonos imagery and a LiDAR-derived DEM, and, then, the results obtained from both data sources are combined to remove inconsistencies. Vosselman (2002) combined LiDAR, plan view, and high-resolution aerial image data to automatically reconstruct 3D buildings. In Jaw and Cheng (2008) buildings are segmented in LiDAR data and refined in an aerial image. Kim and Habib (2009) proposed a method for the automated generation of polyhedral building models for complex structures, starting with the extraction of individual planar patches from the LiDAR point cloud, refining them with image data, and finally generating the polyhedral building model with the refined building patches. Cheng *et al*. (2011) proposed an approach integrating multi-view aerial image and LiDAR data to reconstruct 3D building models. Chen and Zhao (2012) proposed an approach integrating QuickBird imagery and LiDAR-derived nDSM to detect building, in which the nDSM is used for eliminating ground points and the image for detecting the buildings. In Sun and Savalggio (2012), LiDAR data and an orthorectified aerial image were combined for building roof extraction. LiDAR data is used for detecting building roof and providing their approximate outlines, and the orthoimage is used to refine the LiDAR-derived outlines. Other recent papers (e.g. Awrangjeb *et al*. 2013, Li *et al*. 2013, Gilani *et al*. 2015, Guo *et al*. 2016) have reported methods integrating different data source to delineate building roof boundaries.

Building roof boundaries are potentially well defined in image data than in LiDAR data. For example, let us consider a very high-resolution aerial image with a ground sample distance (GSD) of 10 cm and a high-density LiDAR point cloud with 10 points per square metre (i.e. 10 pts./m^2). Consequently, this aerial image provides a point density

10 times greater than the LiDAR point cloud, and, as such, breaklines, like building roof contours, are better defined in the image data. The opposite occurs when the goal is the reconstruction of surfaces with homogeneous texture, like the planar surface of roof faces. Stereophotogrammetric techniques can be used for surface reconstruction, but in case of homogenous texture surface, as is the case of planar surfaces of building roofs, almost no 3D positional information is obtained from a stereoscopic pair of very high-resolution aerial images. On the other hand, LiDAR data supply dense 3D positional information for surface reconstruction, even when the surface has homogeneous texture. Taking also in consideration that LiDAR points have high vertical accuracy (about 10 cm), the extraction of planar building roofs using LiDAR data is potentially more accurate and reliable than using image data. A comprehensive empirical study of the above-discussed properties was presented in Kaartinen *et al*. (2005).

Following the above arguments, the main motivation of this paper is the possibility of refining the contours of the LiDAR-derived building polyhedron by using its well-defined planar roof faces and the corresponding well-defined building roof contour extracted from only one high-resolution aerial image. The proposed method requires only that building roofs are constituted by planar faces and bounded by straight lines. These requirements are found in most common types of roofs, as for example: flat, gable, shed, mansard, gambrel, butterfly, and hip. The main focus of this paper is on a proposed line-based photogrammetric model, which allows the refinement of 3D building roof contours. This paper is organised as follows. Section 2 presents the proposed method. Results are presented and discussed in Section 3. Finally, the paper is finalised in Section 4 presenting some conclusions and future work.

2. Photogrammetric approach for building roof contour refinement

The proposed method is based on two main steps. First, straight lines representing the sides of a selected building roof contour are extracted from the image and projected onto corresponding LiDAR-derived building polyhedron faces by using a line-based photogrammetric model. It is worthy noting that, for each selected building, the straight lines extracted from the image must be matched to corresponding polyhedron roof faces. This correspondence problem can be solved algorithmically or visually. In this paper neither the straight-line extraction nor the matching between straight lines and planar roof faces is accomplished by specific algorithms. Section 2.1 presents the line-based photogrammetric model. Second, the refined contour of the polyhedron is determined by connecting every pair of adjacent projected lines, resulting in a new set of contour vertices. Section 2.2 describes the method for determining the refined contour of the polyhedron.

2.1. *Line-based photogrammetric model*

Figure 1 shows the geometric principle of the proposed method for projecting image-space straight lines onto corresponding building polyhedron faces. For instance, let us consider the polyhedron edge $\overline{A'B'}$ (dashed line in Figure 1) to show how to photogrammetrically refine it. Suppose that the image-space straight-line segment $\overline{ab}$

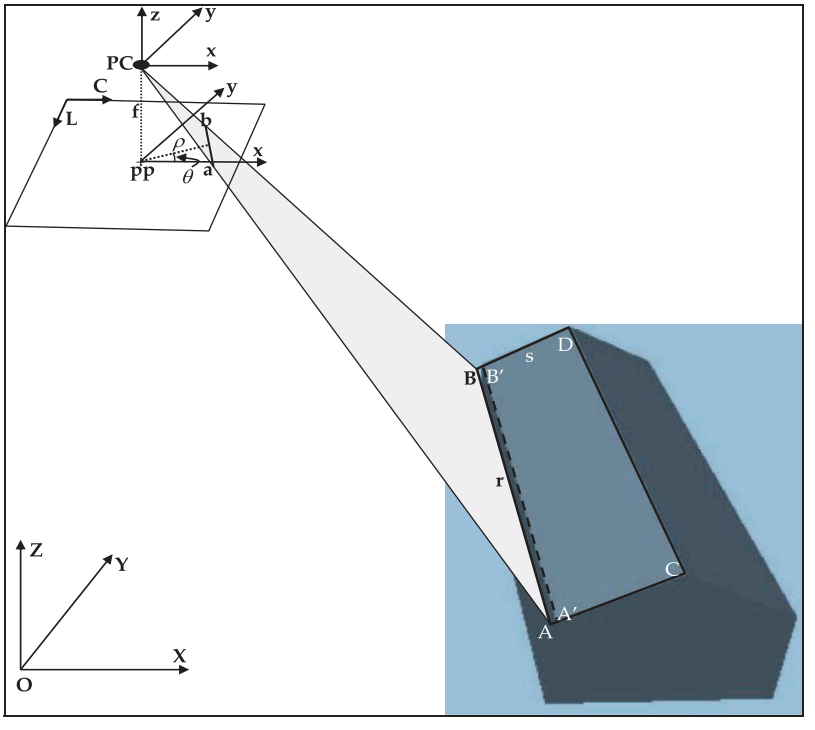

Figure 1. Principle of the proposed photogrammetric method.

corresponds to the polyhedron edge $\overline{A'B'}$. As such, the segment $\overline{ab}$ defines one of the sides of the building representing the polyhedron in the image. Moreover, their end-points or parameters can be measured in the image, manually or by an appropriate algorithm. The projection of the line segment $\overline{ab}$ onto the corresponding building polyhedron face (resulting in the 3D straight-line $\overline{AB}$) is based on the intersection between two planes (Figure 1), as follows:

- Plane defined by the perspective centre (PC) and the line segment $\overline{ab}$
- Plane containing the polyhedron points A′, B′, C, and D

As shown in Figure 1, the intersection of both planes generates the straight line *r* containing the unknown points A and B.

It is possible to demonstrate that the image-space plane defined by the PC and the straight-line segment $\overline{ab}$ can be expressed in the photogrammetric reference system PCxyz (see Figure 1) as follows,

$$-f\cos(\theta)x - f\sin(\theta)y + \rho z = 0 \tag{1}$$

In Equation (1) (see also Figure 1), *f* is the focal length of the camera; θ is the angle between the x-axis and the straight line that contains the principal point (pp) and is perpendicular to the straight line $\overline{ab}$; and ρ is the distance between the pp and the straight line $\overline{ab}$.

Equation (1) shows that the following vector is normal to the image-space plane,

$$\overrightarrow{N_i}=[-f\cos\theta - f\sin\theta\,\rho]^T \tag{2}$$

The vector $\overrightarrow{N_i}$ can be transformed into the object-space reference system (OXYZ) by the following transformation,

$$\overrightarrow{N_0}=R^T\overrightarrow{N_i} \tag{3}$$

In Equation (3), R is the rotation matrix between the PCxyz and OXYZ reference systems. The rotation matrix elements (r_{ij}) are functions of the camera attitude angles κ, ϕ, and ω.

Let n_x, n_y, and n_z be the components of the vector $\overrightarrow{N_0}$ and X_0, Y_0 and Z_0 be the coordinates of the PC in the OXYZ reference system. The equation of the object-space plane (π, Figure 1) that is normal to the vector $\overrightarrow{N_0}$ is given by Equation (4).

$$\begin{bmatrix} n_x \\ n_y \\ n_z \end{bmatrix} x \begin{bmatrix} X-X_0 \\ Y-Y_0 \\ Z-Z_0 \end{bmatrix} = n_x(X-X_0)+n_y(Y-Y_0)+n_z(Z-Z_0)= 0 \tag{4}$$

In Equation (4), 'x' is the inner product operator and X, Y, and Z are the coordinates of a point belonging to the object-space plane.

Equation (4) can be re-written by rearranging and grouping their variables, as follows:

$$A_0X+B_0Y+C_0Z+D_0= 0 \tag{5}$$

In Equation (5), $A_0=n_x$, $B_0=n_y$, $C_0=n_z$ and $D_0= -n_xX_0-n_yY_0-n_zZ_0$.

As A′, B′, C, and D are coplanar points (see Figure 1), the plane equation (Equation (6)) that represents the selected building roof face (onto which the straight-line segment $\overline{ab}$ is projected) can be developed by using three of these points.

$$IX + JY + KZ + L = 0 \tag{6}$$

In Equation (6), I, J, K, and L are the plane equation coefficients. The intersection of planes given by Equations (5) and (6) allows the determination of the straight-line equation (**r**) containing the unknown points A and B (see Figure 1), that is,

$$\begin{aligned} X &= (B_0K - C_0J)t \\ Y &= (C_0I - A_0K)t + \frac{D_0C_0J - D_0B_0K - C_0D_0J + C_0B_0L}{B_0^2K - B_0C_0J} \\ Z &= (A_0J - B_0I)t + \frac{D_0J - B_0L}{B_0K - C_0J} \end{aligned} \tag{7}$$

where, $t \in R$.

2.2. *Determination of the refined building roof contour vertices*

The determination of the refined building contour vertices is accomplished by intersecting straight lines representing building roof contour sides with object-space planes. For example (see Figure 1), the vertex **B** is determined by intersecting the straight line (represented by Equation (7)) containing points **B**′ and **D** (i.e. the projected straight line **s** in Figure 1) with the object-space plane (represented by Equation (6)) containing the

image-space points **a** and **b**. Please note that the main problem here is how to properly select the projected straight line and the object-space plane that allow the determination of each new vertex of the building roof contour.

The refining algorithm takes in consideration that each LiDAR-derived side of the roof contour has only one corresponding projected straight line. The refining algorithm proceeds as follows:

(1) Choose arbitrarily the first side of the LiDAR-derived building roof contour;
(2) Identify the object-space plane (π) that generated the straight line (r) corresponding to the LiDAR derived roof side selected previously in step 1;
(3) Seek in the clockwise direction for the next side of the LiDAR-derived building roof contour; let s be the corresponding object-space straight line generated by the line-based photogrammetric model;
(4) Intersect the plane π with the straight line s to generate a refined building roof contour vertex (B);
(5) If B coincides with the first refined vertex, discard it and stop; otherwise, reset the straight line s to r and return to step 2.

All vertices determined by the above algorithm define the refined building roof contour, and, as such, it should replace the original building roof contour.

3. Results and discussion

The data set used in the experiments is from the city of Curitiba, Brazil. It comprehends one stereoscopic pair of high-resolution aerial images (GSD ~ 0.2 m), along with the interior (focal length, coordinates of the principal point, and lens distortion coefficients) and exterior (attitude and CP coordinates of the camera) orientation parameters, and 3D models of three buildings. Two 3D models were derived for each building, as follows: (1) one from a LiDAR data set (with point density of about 2 pts./m^2) using an in-house software; and (2) another from the stereoscopic pair of aerial images using the Leica Photogrammetry Suite® (LPS) photogrammetric system. The latter is used as the reference 3D building model in the evaluation of the refined 3D building model. The in-house software is based on standard procedures for three-dimensional reconstruction of building roofs, as for example: LiDAR point cloud filtering for separating ground and aboveground points; segmentation of roof planes based on the local homogeneity of normal vectors of the triangulated aboveground points; least squares adjustment of a plane to points of each roof segment; determination of lines of roof ridges by properly intersecting pair of adjacent roof planes; determination of the roof contour polygon based on the analysis of roof discontinuities; finally, the roof contour polygon and all lines of roof ridges are combined to form each polyhedral roof model.

The results obtained using the three test building roofs are presented and analysed below. As the main focus of this paper is on the geometric accuracy of the proposed retracing process of LiDAR-derived building roof contours, straight lines that delimit building roof contours were manually extracted from one aerial image of the available stereoscopic pair. In addition, the matching between each building roof straight line and

the corresponding polyhedron roof face has been also solved visually. To accomplish this matching task, the straight lines that delimit the polyhedron roof faces should be photogrammetrically transformed into the image space and overlaid on the image, thus allowing the visual identification of correspondences between extracted and projected straight lines. Figure 2 shows the hip-like building roof used in the first test.

Table 1 shows the vertex coordinates of the building roof contours derived previously from LiDAR and stereophotogrammetric data and extracted by the proposed method. The building roof contour vertices are in Universe Transverse Mercator (UTM) coordinates (E, N) and in orthometric height (h).

Table 2 shows the discrepancies between the LiDAR-derived and reference building roof contours and between the refined and reference building roof contours. The discrepancy metric is defined as the Euclidian distance between corresponding vertices (V1, V2, V3, and V4) of building roof contours being numerically compared. These discrepancies show that the proposed method allows a clear improvement in the geometric quality of the LiDAR-derived building roof contour. As also shown in Table 2, the Root Mean

Figure 2. Test building 1.

Table 1. Vertex coordinates (in metre) of the LiDAR-derived, refined, and reference building roof contours – test building 1.

	LiDAR-derived building roof contour			Refined building roof contour extracted by the proposed method			Reference building roof contour extracted from stereophotogrammetric data		
Vertices	*E*	*N*	*h*	*E*	*N*	*h*	*E*	*N*	*h*
V_1	675896.5	7188210.7	921.2	675896.3	7188209.9	922.0	675896.5	7188210.1	922.4
V_2	675902.9	7188201.9	923.2	675902.6	7188202.3	923.2	675902.7	7188202.3	922.8
V_3	675910.1	7188207.9	925.8	675909.8	7188207.8	925.0	675909.6	7188207.6	924.4
V_4	675903.7	7188215.9	923.1	675903.5	7188215.4	923.9	675903.3	7188215.1	924.2

Table 2. Discrepancies (in metre) between the LiDAR-derived and reference building roof contours and between the refined and reference building roof contours – test building 1.

Vertices	Discrepancies at the LiDAR-derived building roof contour vertices	Discrepancies at the refined building roof contour vertices
V_1	1.3	0.5
V_2	0.6	0.4
V_3	1.5	0.7
V_4	1.4	0.5
RMSE	1.3	0.5

Square Error (RMSE) shows that the refined building roof contour is significantly (almost twice) more accurate than the LiDAR-derived building roof contour.

The second test uses the hip-like roof showed in Figure 3, which is similar to the one used in the first test.

The vertex coordinates of the building roof contours derived previously from LiDAR and stereophotogrammetric data and extracted by the proposed method are presented in Table 3.

The discrepancies between the LiDAR-derived and reference building roof contours and between the refined and reference building roof contours are shown in Table 4, together with the RMSE for the refined and LiDAR-derived building roof contour vertices. Once again, the refined building roof contour is geometrically better than the LiDAR-derived building roof contour. One can note that the LiDAR-derived roof contour of the test building 2 is less accurate than the LiDAR-derived building roof contour used in the previous test. RMSE values in Table 4 show that the proposed refinement approach was

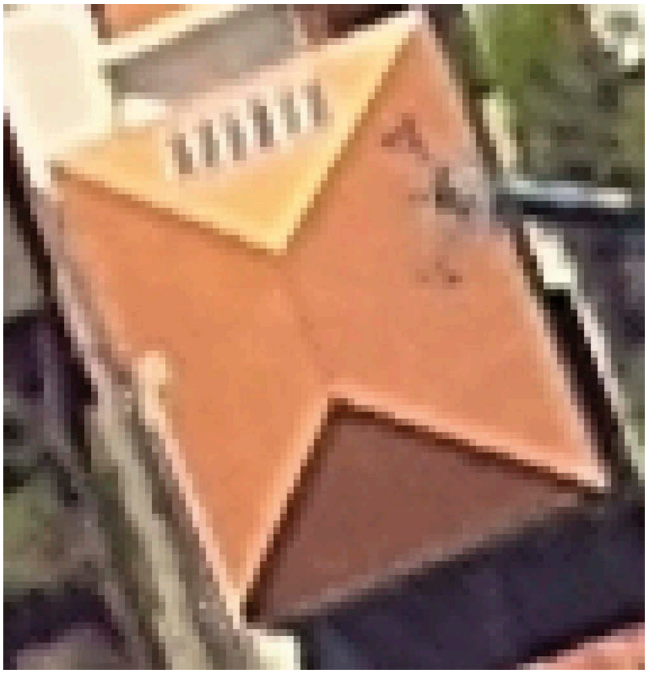

Figure 3. Test building 2.

Table 3. Vertex coordinates (in metre) of the LiDAR-derived, refined, and reference building roof contours – test building 2.

	LiDAR-derived building roof contour			Refined building roof contour extracted by the proposed method			Reference building roof contour extracted from stereophotogrammetric data		
Vertices	*E*	*N*	*h*	*E*	*N*	*h*	*E*	*N*	*h*
V_1	675845.3	7188377.2	924.5	675843.5	7188376.3	923.2	675843.1	7188376.6	924.0
V_2	675855.7	7188384.8	922.3	675854.1	7188383.6	925.1	675854.3	7188383.7	924.1
V_3	675844.9	7188398.0	920.5	675843.7	7188396.5	923.2	675844.4	7188396.9	923.9
V_4	675835.3	7188390.0	924.1	675834.0	7188388.8	924.7	675833.6	7188388.4	924.2

Table 4. Discrepancies (in metre) between the LiDAR-derived and reference building roof contours and between the refined and reference building roof contours – test building 2.

Vertices	Discrepancies at the LiDAR-derived building roof contour vertices	Discrepancies at the refined building roof contour vertices
V_1	2.3	0.9
V_2	2.5	1.0
V_3	3.6	1.1
V_4	2.3	0.7
RMSE	2.7	0.9

able to successfully retrace the LiDAR-derived building roof contour, because the accuracy of the refined building roof contour is about three times better. However, the refined roof contour of the building test 2 (RMSE = 0.5 m) is not as accurate as the refined roof contour of building test 1 (RMSE = 0.9 m).

Figure 4 shows that the building roof used in the third test is much more complex than the building roofs used in the first two tests. It is composed by a main roof branch, which is orthogonally connected to three secondary roof branches. Generally, this building roof is a composite of four gable roofs. The extremity of the central secondary roof branch has fine geometric details that are difficult to model using the available LiDAR point cloud, mainly due to its low point density. Figure 4 also shows the approximate positions of the LiDAR-derived building roof vertices. Particularly, geometric details on the extremity of the central roof branch were coarsely described.

As the roof contour of the test building 3 is defined by many vertices, only the RMSEs of the LiDAR-derived and refined building roof contours will be presented and analysed in the following. Both RMSEs are 1.9 m and 0.7 m, respectively. This means that the refined roof contour is almost three times more accurate than the LiDAR-derived roof contour. Larger discrepancies for both LiDAR-derived and refined roof contours are found at the four vertices located along the extremity of the central roof branch. As already described, these vertices have the worse geometric conditions, and, as a result, larger discrepancies at these vertices might be expected. The smaller discrepancies are found at the right-angle vertices of the main roof branch, which are geometrically defined by large roof planes and long segments of straight lines. These are optimal conditions for determining the building roof contour vertices.

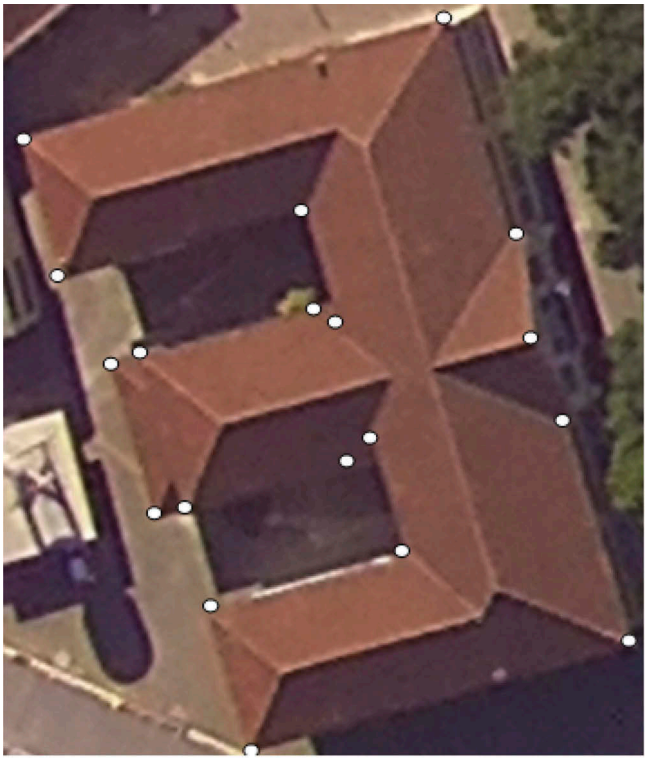

Figure 4. Test building 3 with approximate locations of LiDAR-derived building roof contour vertices.

4. Conclusions and future work

This paper presented a two-step method for solving the proposed problem. First, line-based photogrammetric method is used for projecting straight lines representing building roof sides onto corresponding LiDAR-derived building roof faces. Then, the vertices of the refined building roof contour are determined by properly combining adjacent projected straight lines. The proposed method can be applied for retracing contours of many types of building roofs previously extracted from LiDAR data. Some examples of treatable building roofs are: hip, flat, gable, shed, mansard, gambrel and butterfly. The basic geometric requisites for these types of building roofs are: roof faces must be planar; and the roof contour must be rectilinear.

Three experiments were accomplished to exemplify the method performance. These examples were based on two simple hip-like roofs and one complex building roof that combines several gable roofs. The obtained results are in accordance to the expectation that the integration of LiDAR and photogrammetric data allows a better result to be obtained in the context of building roof contour delineation. In fact, results obtained in the presented tests show that the refined building roof contours were 2–3 times more accurate than the corresponding LiDAR-derived building roof contours. This is especially expected whenever the point density in image data is too higher than the point density in the LiDAR point cloud. In fact, the point density of the test images is about 12 times

higher than the point density of the test LiDAR point cloud used to generate the three building models.

An interesting problem for future study is the development of error models for both the straight line projection and LiDAR-derived building reconstruction processes. These error models would be the basis for verifying beforehand whether a LiDAR-derived building roof side should be replaced by the corresponding projected straight-line segment. This makes sense because in case of weak geometry (e.g. buildings that are distant from the image centre can involve object-space and building roof planes intersecting at small angle), the projected straight line can be less accurate than the corresponding LiDAR-derived straight line. Another direction for future work involves the improvement of the method in order to allow the correction of details not modelled by the LiDAR-based method. Examples of such problem were discussed in the third test. Finally, the level of automation of the proposed method can be significantly improved by using image processing algorithm, like the Hough transform for straight-line extraction from the image, and by developing a matching algorithm for finding correspondences between image-space roof contour straight lines and planar faces of building roof polyhedron.

Acknowledgements

This work was supported by the CNPq (Brazil) under Grant number 304879/2009-6.

Funding

This work was supported by the CNPq (Brazil) under Grant number 304879/2009-6.

ORCID

Aluir Porfírio Dal Poz http://orcid.org/0000-0002-2534-1229

References

Akçay, H.G. and Aksoy, S., 2008. Automatic detection of geospatial objects using multiple hierarchical segmentations. *IEEE Transactions on Geoscience and Remote Sensing*, 46 (7), 2097–2111. doi:10.1109/TGRS.2008.916644

Argyridis, A. and Argialas, D.P., 2016. Building change detection through multi-scale GEOBIA approach by integrating deep belief networks with fuzzy ontologies. *International Journal of Image and Data Fusion*, 7 (2), 148–171.

Awrangjeb, M., Zhang, C., and Fraser, C.S., 2013. Automatic extraction of building roofs using LIDAR data and multispectral imagery. *ISPRS Journal of Photogrammetry and Remote Sensing*, 83, 1–18. doi:10.1016/j.isprsjprs.2013.05.006

Chen, L. and Zhao, S., 2012. Building detection in an urban area using LiDAR data and quickbird imagery. *International Journal of Remote Sensing*, 33 (16), 5135–5148. doi:10.1080/01431161.2012.659355

Chen, Y., *et al*., 2014. Multiscale grid method for detection and reconstruction of building roofs from airborne LiDAR data. *IEEE Journal of Selected Topics in Applied Earth Observations and Remote Sensing*, 7 (10), 4081–4094. doi:10.1109/JSTARS.2014.2306003

Cheng, L., *et al*., 2011. 3D building model reconstruction from multi-view aerial imagery and lidar data. *Photogrammetric Engineering & Remote Sensing*, 77 (2), 125–139. doi:10.14358/PERS.77.2.125

Dennis Dahlke, D., Linkiewicz, M., and Meissner, H., 2015. True 3D building reconstruction: façade, roof and overhang modelling from oblique and vertical aerial imagery. *International Journal of Image and Data Fusion*, 6 (4), 314–329. doi:10.1080/19479832.2015.1071287

Ferraioli, G., 2010. Multichannel InSAR building edge detection. *IEEE Transactions on Geoscience and Remote Sensing*, 48 (3), 1224–1231. doi:10.1109/TGRS.2009.2029338

Fua, P. and Hanson, A.J., 1987. Resegmentation using generic shape: locating general cultural objects. *Pattern Recognition Letters*, 5, 243–252. doi:10.1016/0167-8655(87)90070-5

Galvanin, E.A.S. and Dal Poz, A.P., 2012. Extraction of building roof contours from LiDAR data using a Markov-random-field-based approach. *IEEE Transactions on Geoscience and Remote Sensing*, 50, 981–987. doi:10.1109/TGRS.2011.2163823

Gilani, S.A.N., Awrangjeb, M., and Lu, G., 2015. Fusion of LiDAR data and multispectral imagery for effective building detection based on graph and connected component analysis. *In*: *International archives of photogrammetry, remote sensing and spatial information science*, March 2015 Munich. Amsterdam: ISPRS, 65–72.

Guo, Z., *et al*., 2016. Exploring GIS knowledge to improve building extraction and change detection from VHR imagery in urban areas. *International Journal of Image and Data Fusion*, 7 (1), 42–62. doi:10.1080/19479832.2015.1051138

Haala, N. and Brenner, C., 1999. Extraction of buildings and trees in urban environments. *ISPRS Journal of Photogrammetry and Remote Sensing*, 54, 130–137. doi:10.1016/S0924-2716(99)00010-6

Haala, N. and Kada, M., 2010. An update on automatic 3D building reconstruction. *ISPRS Journal of Photogrammetry and Remote Sensing*, 65 (6), 570–580. doi:10.1016/j.isprsjprs.2010.09.006

Henn, A., *et al*., 2013. Model driven reconstruction of roofs from sparse LIDAR point clouds. *ISPRS Journal of Photogrammetry and Remote Sensing*, 76, 17–29. doi:10.1016/j.isprsjprs.2012.11.004

Jaw, J.J. and Cheng, C.C., 2008. Building roof reconstruction by fusing laser range data and aerial images. *In*: *International archives of photogrammetry, remote sensing and spatial information science*, July 2008 Beijing. Amsterdam: ISPRS, 707–712.

Kaartinen, H., *et al*., 2005. Accuracy of the 3D city model: EuroSDR comparison. *In*: *International archives of photogrammetry, remote sensing and spatial information science*, September 2005 Enschede. Amsterdam: ISPRS, 227–232.

Kim, C. and Habib, A., 2009. Object-based integration of photogrammetric and LiDAR data for automated generation of complex polyhedral building models. *Sensors*, 9, 5679–5701. doi:10.3390/s90705679

Li, Y., *et al*., 2013. An improved building boundary extraction algorithm based on fusion of optical imagery and LiDAR data. *Optik – International Journal for Light and Electron Optics*, 124 (22), 5357–5362. doi:10.1016/j.ijleo.2013.03.045

Matikainen, L., Hyyppä, J., and Hyyppä, H., 2003. Automatic detection of buildings from laser scanner data for map updating. *In*: *International archives of photogrammetry, remote sensing and spatial information science*, October 2003 Dresden. Amsterdam: ISPRS.

Müller, D.S. and Zaum, W., 2005. Robust building detection in aerial images. *In*: *International archives of photogrammetry, remote sensing and spatial information science*, August 2005 Vienna. Amsterdam: ISPRS, 143–148.

Perera, S.N., Nalani, H.A., and Maas, H., 2012. An automated method for 3d roof outline generation and regularization in airbone laser scanner data. *In*: *International archives of photogrammetry, remote sensing and spatial information science*, September 2012 Melbourne. Amsterdam: ISPRS, 281–286.

Rottensteiner, F., *et al*., 2005. Automated delineation of roof planes from LiDAR data. *In*: *International archives of photogrammetry, remote sensing and spatial information science*, September 2005 Vienna. Amsterdam: ISPRS, 221–226.

Sampath, A. and Shan, J., 2007. Building boundary tracing and regularization from airborne LiDAR point clouds. *Photogrammetric Engineering & Remote Sensing*, 73 (7), 805–812. doi:10.14358/PERS.73.7.805

Sampath, A. and Shan, J., 2010. Segmentation and reconstruction of polyhedral building roofs from aerial LiDAR point clouds. *IEEE Transactions on Geoscience and Remote Sensing*, 48 (3), 1554–1567. doi:10.1109/TGRS.2009.2030180

Sirmaçek, B. and Ünsalan, C.A., 2011. A probabilistic framework to detect buildings in aerial and satellite images. *IEEE Transactions on Geoscience and Remote Sensing*, 49 (1), 211–221. doi:10.1109/TGRS.2010.2053713

Sohn, G. and Dowman, I.J., 2003. Building extraction using Lidar DEMs and Ikonos images. *In*: *International archives of photogrammetry, remote sensing and spatial information science*, January 2003 Dresden. Amsterdam: ISPRS.

Sun, S. and Salvaggio, C., 2013. Aerial 3D building detection and modelling from airborne LiDAR point clouds. *IEEE Journal of Selected Topics in Applied Earth Observations and Remote Sensing*, 6 (3), 1440–1449. doi:10.1109/JSTARS.2013.2251457

Sun, S. and Savalggio, C., 2012. Complex building roof detection and strict description from LiDAR data and orthorectified aerial imagery. *In*: *2012 IEEE international geoscience and remote sensing symposium*, July 2012 Munich. Piscataway, NJ: IEEE GRSS, 5466–5469.

Tarsha-Kurdi, F., *et al*., 2006. New approach for automatic detection of buildings in airborne laser scanner data using first echo only. *In*: *International archives of photogrammetry, remote sensing and spatial information science*, September 2006 Bonn. Amsterdam: ISPRS.

Tóvari, D. and Vögtle, T., 2004. Object classification in laserscanning data. *In*: *International archives of photogrammetry, remote sensing and spatial information science*, July 2004 Istanbul. Amsterdam: ISPRS, 45–49.

Vosselman, G., 2002. Fusion of laser scanning data, maps, and aerial photographs for building reconstruction. *In*: *IEEE international symposium on geosciences and remote sensing*, June 2002 Toronto. Piscataway, NJ: IEEE, 85–88.

Wei, S., 2008. Building boundary extraction based on LiDAR point clouds data. *In*: *International archives of photogrammetry, remote sensing and spatial information science*, July 2008 Beijing. Amsterdam: ISPRS, 157–162.